

# Sequential Registration-Based Segmentation of the Prostate Gland in MR Image Volumes

Farzad Khalvati<sup>1,2</sup> · Aryan Salmanpour<sup>3</sup> · Shahryar Rahnamayan<sup>3</sup> · Masoom A. Haider<sup>1,2</sup> · H. R. Tizhoosh<sup>4</sup>

© Society for Imaging Informatics in Medicine 2015

**Abstract** Accurate and fast segmentation and volume estimation of the prostate gland in magnetic resonance (MR) images are necessary steps in the diagnosis, treatment, and monitoring of prostate cancer. This paper presents an algorithm for the prostate gland volume estimation based on the semi-automated segmentation of individual slices in T2-weighted MR image sequences. The proposed *sequential registration-based segmentation* (SRS) algorithm, which was inspired by the clinical workflow during medical image contouring, relies on inter-slice image registration and user interaction/correction to segment the prostate gland without the use of an anatomical atlas. It automatically generates contours for each slice using a registration algorithm, provided that the user edits and approves the marking in some previous slices. We conducted comprehensive experiments to measure the performance of the proposed algorithm using three registration methods (i.e., rigid, affine, and nonrigid). Five radiation oncologists participated in the study where they contoured the prostate MR (T2-weighted) images of 15 patients both manually and using the SRS algorithm. Compared to the manual segmentation, on average, the SRS algorithm reduced the contouring time by 62 % (a speedup factor of 2.64×) while

maintaining the segmentation accuracy at the same level as the intra-user agreement level (i.e., Dice similarity coefficient of 91 versus 90 %). The proposed algorithm exploits the inter-slice similarity of volumetric MR image series to achieve highly accurate results while significantly reducing the contouring time.

**Keywords** Image registration · Prostate segmentation · Magnetic resonance imaging · Prostate volume

## Introduction

Prostate cancer is the most common cancer in men. One in six men in Canada is diagnosed with prostate cancer during their lifetime [1]. In most cases, however, the diagnosis of prostate cancer usually leads to active monitoring of tumor growth for a long period of time. A potential treatment may include surgery or radiation therapy. In all cases of diagnosis, treatment and monitoring of prostate cancer, accurate localization and segmentation of the prostate gland and estimation of prostate gland volume in images may be required. Although CT images are generally used for radiation therapy, in many cases, however, MR images are also used for accurate image segmentation because MR imaging is a safer and less invasive method compared to CT scans. As well, the use of MRI could also potentially reduce inter-user variability [2]. Recent studies show that MR images can be used for dose calculation in cancer treatment, which might lead to the complete elimination of the requirement for CT [3, 4].

In order to estimate the volume of the prostate gland, each slice of the volume dataset has to be marked so the boundary of the prostate gland can be labeled. Manual segmentation of the prostate gland is a tedious task as the contouring process of a patient's volume dataset can take several minutes. The long

---

✉ Farzad Khalvati  
farzad.khalvati@sri.utoronto.ca

<sup>1</sup> Department of Medical Imaging, University of Toronto, Toronto, ON, Canada

<sup>2</sup> Physical Sciences Platform, Sunnybrook Research Institute, Toronto, ON, Canada

<sup>3</sup> Department of Electrical, Computer and Software Engineering, University of Ontario Institute of Technology, Oshawa, ON, Canada

<sup>4</sup> Centre for Bioengineering and Biotechnology, University of Waterloo, Waterloo, ON, Canada

time required to process the volume datasets of prostate imposes a serious burden on the healthcare system and prevents timely patient access to proper care. The availability of a segmentation algorithm that reduces the time spent manually contouring the prostate in the clinical workflow is essential and could translate to reduced cost.

The aim of the current study was to develop an algorithm that exploits inter-slice similarity to segment the prostate gland in MR images. Our proposed algorithm was inspired by the clinical workflow during medical image contouring where a clinician usually inspects the automatic or semi-automatic generation of contours to correct and approve them if necessary (e.g., therapy planning). Our algorithm benefits from the inter-slice similarity of images in a volume dataset to propagate a given label (i.e., the segmentation result) to neighboring slices using image registration.

The outline of the remainder of this paper is as follows: In the “[Related Work](#)” section, the related work on the segmentation of prostate images is presented. In the “[Proposed Algorithm](#)” section, we present our proposed algorithm for semi-automatic segmentation of the prostate gland in MR images. “[Materials and Results](#)” and “[Discussion](#)” sections present the performance results and the discussion for the proposed algorithm, respectively. Finally, the “[Conclusion](#)” section concludes the paper.

## Related Work

In terms of related work, our algorithm can be compared to atlas-based segmentation (ABS) algorithms [5–9], which are a class of popular approaches in the literature for prostate segmentation. Briefly, this method involves contouring the desired anatomy (i.e., prostate) by an expert user (or a clinician) and storing the original images with the corresponding labels (i.e., segmented binary image) in a database known as an “atlas”. To segment the prostate in a target image, all of the images in the atlas are registered to the target image using an image registration method. The registered images in the atlas are then compared to the target image using an image similarity matching technique to find the most similar registered image in the atlas. Finally, a segmented image is produced by applying the image transformation function to the segmented binary image (label) that corresponds to the most similar image in the atlas. Different variations of ABS algorithms have been proposed to increase the accuracy of the results and/or reduce the computational cost. In the following, we review several methods from related work.

Klein et al. [5] presented a semi-automatic algorithm based on atlas matching for the segmentation of the prostate gland in MR images. The algorithm used an affine followed by a nonrigid registration method to register all of the images in the atlas with the target image, and then, the most similar

registered images to the target image were selected. The corresponding image transformations were applied to the original segmented images (or labels) to produce the registered labels which were then averaged together and thresholded to generate the final label. In another study, Klein et al. [6] presented an improved version of their previous method [5] in which the registered labels were fused using majority voting and simultaneous truth and performance level estimation (STAPLE) algorithm [10] to generate a consensus label. Dowling et al. [7] proposed a probabilistic atlas-based method where a volume dataset was selected as the initial atlas. The remaining volume datasets with labels were registered twice against the initial atlas via rigid and affine transformations and then using rigid, affine, and nonrigid transformations. A new atlas was generated at the end of each step by averaging the registered images and labels. To segment a target image, the average atlas was registered against it using affine and nonrigid registration methods. The transformation was then applied to the probability map of the prostate and the result was thresholded to generate the result label. Langerak et al. [8] proposed a multi-atlas-based segmentation method for prostate MR images based on an iterative label fusion approach, which was somewhat similar to [6]. First, all of the atlas images were registered against the target image to obtain a set of registered labels, and the registered labels were then fused together using a weighted majority voting method. Next, the overlap of each contour was calculated against the fused label, and labels with low overlaps were dropped and the fused labels were recalculated. Martin et al. [9] proposed a probabilistic atlas-based segmentation method for prostate MR images. The atlas was created by registering images with a manually picked reference image. Next, a mean image was created by averaging all of the registered images. Each image was registered against the mean image to produce a deformed label of the image. The deformed labels were then averaged to generate a probability map of the labels. To segment an image, the mean image was registered to it and the probability map of the labels was deformed using the registration transform. The result label was modified using a deformable model to better match the prostate boundaries.

Cheng et al. [11] proposed two registration guided methods for semi-automatic segmentation of the prostate gland in MR images. In the first method, the user manually contours the base, middle, and apex slices on the three planes (axial, sagittal, and coronal). A nonrigid registration propagates the manual contours from the middle slice toward the base and apex and vice versa depending on the distance from the base and apex. In the second method, before applying the registration, the images are first filtered to remove speckle noise and enhance the edge map of the image. It also uses a fuzzy C-means clustering method to decompose the image into different fuzzy-C classes. The result of the registration (deformed binary mask) is used to combine these classes of the image into a

single binary mask, and then, morphology operations (dilation and erosion) are applied to refine the segmentation result. The algorithm presented in [11] is similar to the SRS algorithm proposed in this paper where both use inter-slice registration to propagate manual contours throughout the prostate volume. One difference is that the method in [11] only uses nonrigid registration with post-processing where the SRS algorithm uses rigid, affine, and nonrigid registrations with no post-processing to evaluate the performance of the algorithm. As it will be seen in “Materials and Results”, the SRS algorithm could achieve an accuracy comparable to the intra-user agreement using rigid registration with no post-processing which requires much less computational time compared to the approach used in [11].

In the clinical workflow for therapy, it is the norm that automatically or semi-automatically generated labels are examined and corrected by a clinician such as a radiation oncologist. The clinical ramifications of not checking contours include missing a target (less effective therapy) or increased toxicity if the target is over-contoured. The Radiation Therapy Oncology Group (RTOG) recommends contouring guidelines for different organs/cases [12]. In all cases, it is assumed that a clinician is responsible for contouring, rather than an automatic segmentation algorithm.

Our proposed algorithm was inspired by clinical workflows for monitoring and treatment of prostate cancer where in the former, the volume estimation of the prostate gland is used for surveillance of the disease (e.g., PSA density calculation) and in the latter, the precise segmentation of the prostate gland in all slices are required for therapy planning, in which case the clinician is responsible for the segmentation results. Instead of using a pre-generated atlas which is costly to create, the initial labels are generated and/or corrected by an expert user on the fly, before producing the labels of the remaining images in the volume dataset. Our results show that using expert knowledge during the segmentation process leads to an average accuracy of 91 % Dice similarity coefficient (DSC), which is similar to the intra-user agreement level (i.e., 90 % DSC) while reducing the overall contouring time by 62 %.

In this paper, we propose a sequential registration-based segmentation (SRS) algorithm for prostate MRI. Using the SRS algorithm, the user initializes the segmentation by contouring the first slice. The SRS algorithm then generates the result for the next slice(s). Depending on the configuration, the user may choose to correct the segmentation result for each slice or they may skip one or more slices before contouring the next slice. We evaluate and report the speedup factors for the SRS algorithm with user initialization and correction compared to manual contouring of the same datasets. This gives a clear picture of the effectiveness of the algorithm in practice. For evaluation purposes, the manual contouring of five clinicians was used where intra-user variability was reported and used as a baseline for performance evaluation of the SRS algorithm.

## Proposed Algorithm

The contouring of medical images for prostate cancer is usually performed for prostate cancer detection and monitoring [13] and treatment planning for radiation therapy [14]. During the monitoring of the disease, prostate volume estimation is used for PSA density calculation, which is a biomarker for prostate cancer diagnosis. In treatment planning, the generated labels are used for dose calculations and actual radiation therapy, so the clinician usually contours the slices one by one to ensure high accuracy of individual labels. Planning is generally performed using CT scans, but the segmentation and registration of MR images may also be required when it is desirable to fuse two modalities. Our proposed algorithm, i.e., the sequential registration-based segmentation algorithm or SRS, was inspired by these clinical workflows where in diagnosis and monitoring the disease, the volume of prostate cancer can be estimated with minimal user intervention and in treatment planning, each slice segmentation result is verified and corrected by the clinician to ensure the accuracy of contours. In both scenarios, the SRS algorithm relies on the user intervention to generate the label of a given slice. The amount of user intervention can be chosen depending on the clinical workflow. For treatment planning, the clinician would choose to edit/correct any generated label whereas for diagnosis and monitoring, they may choose to skip one or more slices before manually contouring a slice. As it will be discussed in the “Results for the SRS Algorithm” section, the SRS algorithm can produce acceptable segmentation accuracy while it speeds up the segmentation with respect to manual contouring significantly.

The images in an atlas used by ABS methods may belong to different series, different studies, or even different patients. ABS methods generally assume that registration will eliminate the differences between images (i.e., atlas images and the target image). However, MR images contain a variety of details that can make the registration task difficult if the images belong to different patient data. On the other hand, images in a volume dataset share a large amount of information, especially those that are adjacent to each other, because they represent different cross-sections of the same volumetric object. In this scenario, image registration should yield a better result without any need for a large atlas of images. This is the underlying concept of the SRS algorithm proposed in this paper.

The proposed algorithm registers images in a given volume dataset against each other, thereby eliminating the need to use an atlas. It can use rigid, affine [15, 16], or nonrigid registration methods to generate labels. For the nonrigid registration, demon algorithm [17] was used since it is a well-known nonrigid registration algorithm that has been successfully used in registering medical images in different modalities [18, 19]. In our experiments, an open-source implementation [20] was used for rigid, affine, and demon registration algorithms.

The proposed SRS algorithm is presented in two formats. In the first format, which is suitable for treatment planning (“SRS Algorithm with Post-editing”), it is assumed that the expert user corrects the result for each slice. In the second format, which is suitable for prostate volume estimation used for diagnosis and monitoring (“SRS Algorithm Without Post-editing”), the expert user may skip contouring one or a few slices between a given pair of slices that have been contoured by the user.

### SRS Algorithm With Post-editing

In this configuration, suitable for treatment planning, it is assumed that the user will correct any segmentation result before moving to the next slice. We consider a set of  $n+1$  slices of the prostate gland in an MR sequence  $\{I_K\}, K=0, \dots, n$  with a slice thickness of  $Th$ . The SRS algorithm can be summarized as follows:

1. Initialization: An expert user contours the prostate for  $I_0$  in a MR image sequence, which is the first slice (i.e., base slice). This yields the label for the first slice  $L_0$ . The algorithm finds the ROI based on the user label around the prostate. Based on an assumption that the prostate gland boundary in the second slice is probably larger than the one in the base slice, the ROI is slightly enlarged (i.e., by 30 %) for use in the next slice  $I_1$  of the MR image sequence<sup>1</sup>. The largest ROI of the two is used when registering each slice with the next.
2. Image registration: At each step  $i-1$ , the current slice,  $I_{i-1}$ , is registered with the next,  $I_i$ , using a registration method as follows:

$$T_{i-1} = \text{Reg}(I_{i-1}, I_i) \quad (1)$$

where  $\text{Reg}$  is a registration method (rigid, affine, or nonrigid) and  $i \in \{1, \dots, n\}$ . The computed registration transformation,  $T_{i-1}$ , is then applied to the label of the current slice,  $L_{i-1}$  to generate the registered deformed label,  $L_i^r$ , which is the auto-generated label for the next slice,  $I_i$ .

$$L_i^r = T_{i-1}(L_{i-1}) \quad (2)$$

3. User intervention: In this step, the expert user modifies label  $L_i^r$  generated for slice  $I_i$ , if necessary. The edited (corrected) label for slice  $I_i$  is  $L_i$ . A new ROI is built after

the user corrects the current slice. A linear interpolation method is used to find an ROI for  $I_{i+1}$  in the image sequence based on the ROIs of  $I_i$  and  $I_{i-1}$ .

4. Repeat steps 2 and 3: The algorithm continues by repeating steps 2 and 3 until the end of the image sequence (i.e.,  $i=n$ ).

### SRS Algorithm Without Post-editing

In this configuration (suitable for prostate volume estimation used for diagnosis and monitoring), the user may skip  $z$  slices before contouring a slice manually. We consider a set of  $n+1$  slices of the prostate gland in a MR sequence  $\{I_K\}, K=0, \dots, n$  with a slice thickness of  $Th$ . The SRS algorithm can be summarized as follows:

1. Initialization: This step is similar to step 1 in SRS with post-editing (“SRS Algorithm with Post-editing”).
2. Set  $i=0$ .
3. Starting from  $I_j$  and moving forward by  $z$  slice (i.e.,  $I_{j+z}$ ), each image is registered to the next image as follows:

$$T_{j-1}^{r1} = \text{Reg}(I_{j-1}, I_j) \quad (3)$$

where  $\text{Reg}$  is a registration method (rigid, affine, or nonrigid) and  $j \in \{i+1, \dots, i+z\}$ . At each step  $j$ , the computed registration transformation,  $T_{j-1}^{r1}$  is applied to slice  $I_{j-1}$  and its label  $L_{j-1}$ , which generates the registered image,  $I_j^{r1}$ , and the deformed label,  $L_j^{r1}$  which is the result label for the next slice,  $I_j$ :

$$I_j^{r1} = T_{j-1}^{r1}(I_{j-1}) \quad (4)$$

$$L_j^{r1} = T_{j-1}^{r1}(L_{j-1}^{r1}) \quad (5)$$

4. Increment  $i$ :  $i=i+z+1$ .
5. The expert user contours the prostate in slice  $I_i$  manually.
6. Repeat steps 3 and 4: The algorithm continues by repeating steps 3 and 4 until the end of the image sequence (i.e.,  $i>=n$ ).

## Materials and Results

This section presents the test images used in the experiments and the performance evaluation measures. All three registration methods (i.e., rigid, affine, and nonrigid) were used to generate results for MR images using SRS both with and without post-editing.

<sup>1</sup> The entire image is not used as the ROI because registration usually gives a poor result in this case. Therefore, the ROI is usually limited by the user before the registration starts [5, 6]. SRS was designed specifically for the prostate gland where the cross section of the prostate is small at the base and the apex and it usually becomes larger as we approach the mid-gland region. We used a slightly enlarged ROI because the second slice was more likely to contain a larger portion of the prostate than the first slice when we navigated from the base to the apex. Thus, the second slice might not cover the whole prostate if we use the same ROI. The 30 % ROI enlargement was selected based on the empirical data.

### Prostate MR Images

The MR images (T2-weighted with endorectal coil) used in this study were derived from an online database (<http://prostateMRimageDatabase.com>), which contains MR volume datasets provided by Brigham and Women’s Hospital, the National Center for Image-Guided Therapy, and Harvard Medical School. The database was created with proper Internal Review Board (IRB) approval. The pulse sequence groups in the Digital Imaging and Communications in Medicine (DICOM) headers of the T2-weighted images were marked as fast relaxation fast spin echo-accelerated (FRFSE-XL). This dataset contained images with the slice thickness of 3 mm and varying contrast levels and signal-to-noise characteristics. All of the images were captured with a depth of 16 bits and with 512×512 pixel size. Complete descriptions of the 15 MRI volume datasets considered in the current study are provided in Table 1. Five radiation oncologists manually contoured the MR images for all 15 patients. The same clinicians also edited the segmentation results in post-editing configuration as described in “SRS Algorithm with Post-editing.” The corrected results were compared to the initial manual segmentation results to calculate intra-user variability (or agreement). There were 2 weeks gap between the manual and semi-automatic segmentation experiments. To generate ground-truth segmentations, the manual contours of all five experts were combined using the STAPLE algorithm [10]. For each slice, this produced the consensus contour which was then used as the ground truth to evaluate the performance of the SRS algorithm. The image dataset in DICOM format and manual markings were provided by Segasist Technologies. The same dataset has been a part of multiple algorithm and software validation processes as reported in the literature [21, 22].

### Volume Accuracy

The accuracy of slices was measured by comparing the semi-automatically generated labels with the ground-truth images using Dice similarity coefficient (DSC), which is defined as:

$$DSC = \frac{2|B_g \cap B_s|}{|B_g| + |B_s|} \tag{6}$$

**Table 1** Description of the prostate MR images used in terms of their dimensions (pixels and mm), slice thickness (mm), and total number of slices per volume dataset where the prostate was visible for segmentation ( $N$ )

Total studies	Dimensions (pixels)	Dimensions (mm)	Thickness (mm)	Slices per study
11	512×512	150×150	3	11≤N≤17
1	512×512	160×160	3	13
3	512×512	180×180	3	12≤N≤22

where  $B_g$  and  $B_s$  are ground-truth and semi-automatically generated labels, respectively.  $\cap$  represents the shared information in the two binary images. To calculate the volume accuracy, we used DSC (Eq. 6) to calculate the DSC over the entire 3D prostate.

### Estimation of the Prostate Volume

After the slices of a MR volume dataset have been auto-segmented or manually contoured, the area of each slice,

$A = \{A_i, |i \in \{1, \dots, n\}\}$ , is calculated, where  $n$  is the number of slices in a volume dataset where a portion of the prostate is visible. The estimated volume of the prostate in each volume dataset or image sequence is then calculated based on  $A_i$  and the slice thickness  $Th$  as follows [23]:

$$V = Th \times \left( \frac{A_1 + A_N}{3} + \sum_{i=2}^{N-1} A_i \right) \tag{7}$$

In this calculation, it is assumed that the start point (base) and the end point (apex) of the prostate have a distance of  $Th$  from the adjacent slices, meaning that there are two cone-shaped volumes with  $Th$  as height and  $A_1$  and  $A_n$  as bases.

### Volume Ratio

Volume ratio is a measure which indicates how much the calculated volume of the prostate is deviated from that of ground-truth contours.

$$V_{Ratio}(\%) = \frac{\min(V_s \cdot V_g)}{\max(V_s \cdot V_g)} \times 100 \tag{8}$$

where  $V_s$  and  $V_g$  are the volume values for the SRS algorithm results and the ground truth, respectively. In both cases, the volume was calculated using Eq. 7.

### Mean and Maximum Absolute Distances

For each point on the auto-segmentation result, we measured the distance from the corresponding point on the ground-truth label to calculate the mean absolute distance (MAD) and maximum absolute distance (MAXD).

### Results for the SRS Algorithm

We calculated the intra-user agreement (or variability) for each user on 15 patients’ prostate MR images. Table 2 shows the intra-user agreement results. We used intra-user agreement as a baseline to determine the optimal configuration for the SRS algorithm in which the accuracy of segmentation is comparable to the intra-user agreement level where significant speedups are achieved.

**Table 2** Average intra-user agreement results ( $\pm$ standard deviation) for 5 users for 15 datasets of prostate MR, which includes DSC for the entire volume (%), volume ratio, MAD (mm), and MAXD (mm)

Volume (DSC) (%)	Volume (ratio) (%)	MAD (mm)	MAXD (mm)
89.82 $\pm$ 2.42	89.47 $\pm$ 7.37	1.70 $\pm$ 1.08	4.39 $\pm$ 2.26

In the SRS algorithm without post-editing (“SRS algorithm Without Post-editing”), the number of unedited slices can be between 1 and 5. The corresponding results in Tables 3, 4, and 5 are referred to as “Unedited  $i$ ” where  $i$  represents the number of unedited slices in between any two slices that have been manually contoured. For the SRS algorithm with post-editing (“SRS algorithm with Post-editing”), all the segmentation results were edited. The corresponding results are shown as “Unedited 0”.

Tables 3, 4, and 5 summarize the average results for the SRS algorithm using rigid, affine, and nonrigid registration methods. For each registration algorithm, the results are calculated for different configurations from the case where any segmentation result is edited and corrected (i.e., Unedited 0) to the one that between any two manual segmentations, there are five slices for which, the segmentation result has not been edited (i.e., “Unedited 5”). For each case, the DSC for the entire 3D prostate in MR images, volume ratio, MAD, and MAXD measures are reported. In addition, the amount of timesaving as well as the speedup factor for each configuration is reported. The timesaving and speedup are measured by comparing the SRS algorithm for a volume set with respect to the manual segmentation of the same volume set. Each configuration was calculated for five different expert users and the results were averaged.

It is observed that the average intra-user agreement for volume DSC and ratio were 89.82 and 89.47 %, respectively. All three registration methods yielded volume DSCs at the level of the intra-user agreement level with “Unedited 3” configuration. The corresponding speedup factors for rigid, affine, and nonrigid registration methods were 3.33 $\times$ , 2.72 $\times$ , and 1.64 $\times$ , respectively. Since all three registration methods meet the intra-user agreement threshold, it is obvious that rigid

registration would be preferred due to higher speedup achieved. With respect to volume ratio, it is observed that rigid registration with “Unedited 2” is able to produce an accuracy of 90.65 % which is comparable to the intra-user agreement of 89.47 % leading to speedup factor of 2.64 $\times$ . Figures 1 and 2 show a sample prostate MR volume dataset and the corresponding segmentation result for one user.

## Discussion

The contouring of medical images is a major part of diagnosis, active surveillance, and treatment planning, but it faces a major challenge because manual contouring is a tedious task and it requires a significant time commitment by radiation oncologists. The aims of auto-segmentation tools are to reduce the contouring time (higher efficiency) by generating labels that require less user intervention in terms of editing or corrections. The SRS algorithm was designed with the typical clinical workflow in mind where the expert user interacts with the segmentation algorithm to improve the accuracy. It is based on the inter-slice registration of MR images where the user can correct all slices or skip one or more slices in order to complete the segmentation of the entire volume. This means that based on the required accuracy, more slices can be skipped by the user to achieve a higher speedup factor.

On the other hand, intra-user variability (or agreement) is a well-known phenomenon in medical image contouring caused by the inherent complexity of medical images and the vagueness of the anatomical boundaries in such images. It is understood that a segmentation accuracy similar to intra-user agreement level is assumed acceptable by the expert user. In this paper, we ran different experiments with the SRS algorithm where multiple configurations of the algorithm were used. We also used three registration methods (rigid, affine, and nonrigid) to propagate the user-generated labels through the remaining slices in the volume. The speedup was measured by comparing the amount of manual contouring time for the entire volume versus the SRS algorithm where the user contours/

**Table 3** Prostate segmentation average results ( $\pm$ standard deviation) using the SRS algorithm with rigid registration for 15 patients contoured by 5 users, which includes DSC for the entire volume (%),

Unedited slices	Volume (DSC) (%)	Volume (ratio) (%)	MAD (mm)	MAXD (mm)	Timesaving (%)	Speedup
Unedited 0	94.35 $\pm$ 7.30	91.38 $\pm$ 4.46	1.08 $\pm$ 0.42	3.39 $\pm$ 0.88	27.46	1.38 $\times$
Unedited 1	92.73 $\pm$ 7.76	91.33 $\pm$ 5.04	1.39 $\pm$ 0.43	3.95 $\pm$ 0.92	46.56	1.87 $\times$
Unedited 2	90.96 $\pm$ 12.36	90.65 $\pm$ 5.10	1.79 $\pm$ 0.46	4.63 $\pm$ 0.89	62.19	2.64 $\times$
Unedited 3	89.31 $\pm$ 15.44	88.42 $\pm$ 5.96	2.26 $\pm$ 0.52	5.56 $\pm$ 0.96	69.96	3.33 $\times$
Unedited 4	85.15 $\pm$ 17.17	83.93 $\pm$ 7.67	2.69 $\pm$ 0.67	6.33 $\pm$ 1.11	74.13	3.87 $\times$
Unedited 5	77.15 $\pm$ 18.62	80.50 $\pm$ 9.62	3.31 $\pm$ 0.87	7.41 $\pm$ 1.35	77.73	4.49 $\times$

volume ratio, MAD (mm), MAXD (mm), timesaving (%), and speedup factor. “ $i$ ” in “Unedited  $i$ ” that represents the number of unedited slices in between any two slices that have been manually contoured

**Table 4** Prostate segmentation average results ( $\pm$ standard deviation) using the SRS algorithm with affine registration for 15 patients contoured by 5 users, which includes DSC for entire volume (%), volume ratio, MAD

(mm), MAXD (mm), timesaving (%), and speedup factor. “*i*” in “Unedited *i*” represents the number of unedited slices in between any two slices that have been manually contoured

Unedited slices	Volume (DSC) (%)	Volume (ratio) (%)	MAD (mm)	MAXD (mm)	Timesaving (%)	Speedup
Unedited 0	94.35 $\pm$ 7.30	91.38 $\pm$ 4.46	1.08 $\pm$ 0.42	3.39 $\pm$ 0.88	17.82	1.22 $\times$
Unedited 1	92.86 $\pm$ 7.57	91.06 $\pm$ 4.95	1.37 $\pm$ 0.45	3.95 $\pm$ 0.95	41.80	1.72 $\times$
Unedited 2	91.39 $\pm$ 11.07	89.99 $\pm$ 5.32	1.72 $\pm$ 0.49	4.57 $\pm$ 0.98	56.08	2.28 $\times$
Unedited 3	89.94 $\pm$ 13.30	87.85 $\pm$ 6.46	2.11 $\pm$ 0.56	5.41 $\pm$ 1.13	63.27	2.72 $\times$
Unedited 4	86.59 $\pm$ 14.40	83.81 $\pm$ 8.06	2.47 $\pm$ 0.69	6.11 $\pm$ 1.31	67.10	3.04 $\times$
Unedited 5	78.61 $\pm$ 15.35	79.21 $\pm$ 10.09	3.01 $\pm$ 0.90	6.08 $\pm$ 1.39	70.70	3.41 $\times$

corrects some slices and the SRS algorithm segments the remaining slices.

The optimal configuration of the SRS algorithm is the one that yields an accuracy, using a given measure, similar to the intra-user agreement level. It is observed that depending on the accuracy measure, the optimal configuration of the SRS algorithm differs. Figures 3 and 4 show the average volume DSCs and volume ratios with respect to different SRS configurations. If the volume DSC is considered, the intra-user agreement is 89.82 %. To achieve an accuracy similar to this level, all three registration methods require Unedited 3 configuration, which yields volume DSCs of 89.31, 89.94, and 90.58 %, for rigid, affine, and nonrigid registration methods, respectively. The corresponding speedup factors were 3.33 $\times$ , 2.72 $\times$ , and 1.64 $\times$ , respectively.

If volume ratio is considered, the intra-user agreement is 89.47 %. It is seen that rigid registration with Unedited 2 configuration is able to achieve volume ratio of 90.65 %, which is comparable to intra-user agreement of 88.47 % while yielding a speedup factor of 2.64 $\times$ . Volume number is used in PSA density calculation. Therefore, the high volume ratio of the SRS algorithm means it can be used in such a calculation. The speedup factor of 2.64 $\times$  is equal to 62 % timesaving, a significant amount of time-reduction in clinical settings, translating to higher patient throughput in healthcare system.

As it is seen from Fig. 4, rigid registration yields the best results for volume ratio. This may be due to the fact that the

volume ratio only considers the volume number and ignores the actual overlap between two contours. Nevertheless, for the purpose of PSA density calculation, the volume number may suffice in practice.

For therapy planning where the user chooses to edit the segmentation result of the SRS algorithm for any given slice (SRS with post-editing), the rigid registration still yields a speedup factor of 1.38 $\times$ , a timesaving of 27 % which could translate to reduced cost of treatment.

Figure 5 presents the speedup factors for all three registration methods with different SRS configurations. As it is seen, the rigid registration yields higher speedup factors compared to affine and nonrigid because of lower computational time. It must be noted that the SRS algorithm was implemented in Matlab (TM). Therefore, the speedup factors presented here can be seen as the lower bound. If the SRS algorithm is implemented in C++ or GPUs, it is anticipated that the computational time be negligible compared to the manual contouring time. This would mean that the speedup factor for all three registration methods would become the same (Fig. 5, the “ideal” curve).

**Conclusion**

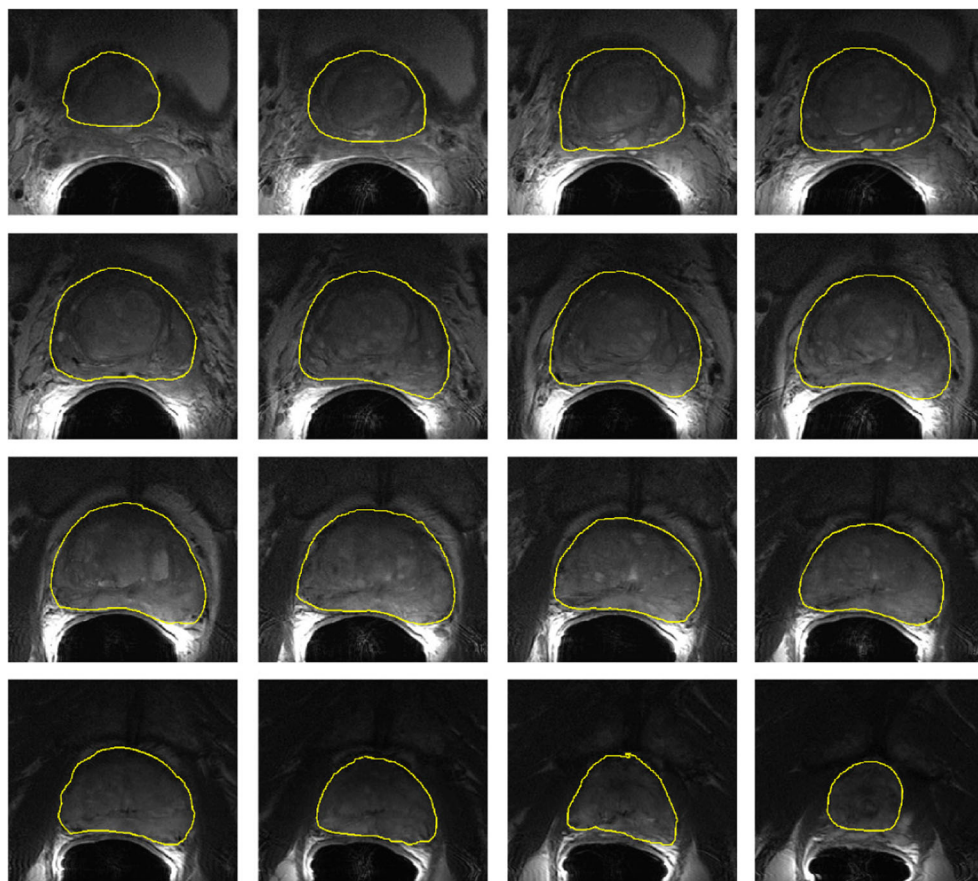
In this paper, we presented an algorithm for segmenting the prostate gland in T2-weighted MR images. The proposed algorithm was inspired by the clinical workflow where an expert

**Table 5** Prostate segmentation average results ( $\pm$ standard deviation) using the SRS algorithm with nonrigid registration for 15 patients contoured by 5 users, which includes DSC for the entire volume (%),

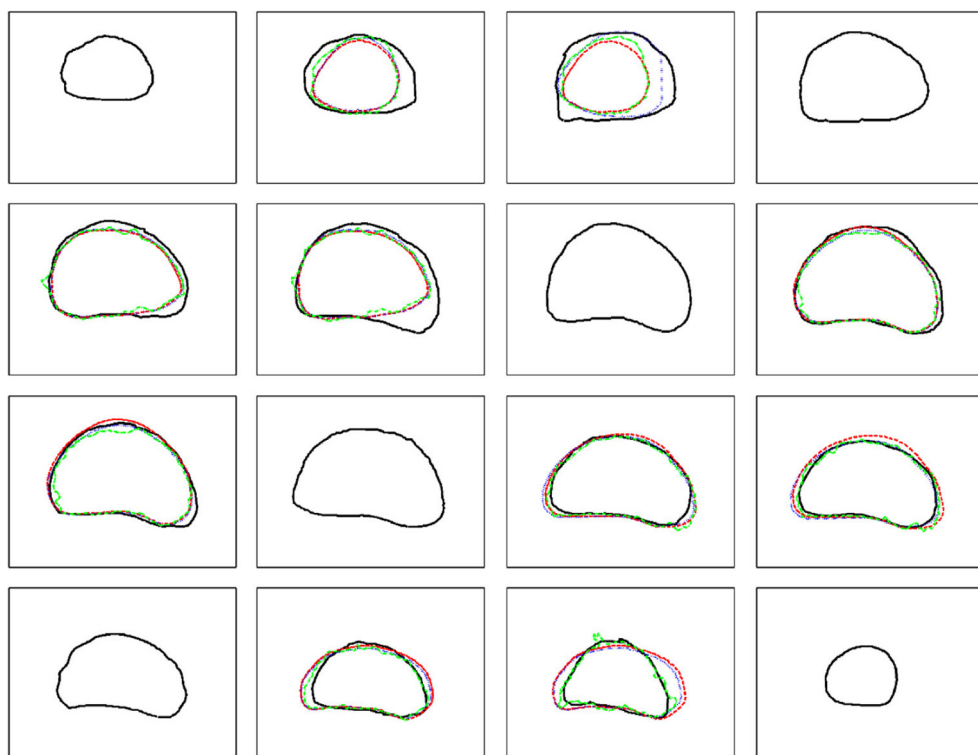
volume ratio, MAD (mm), MAXD (mm), timesaving (%), and speedup factor. “*i*” in “Unedited *i*” represents the number of unedited slices in between any two slices that have been manually contoured

Unedited slices	Volume (DSC) (%)	Volume (ratio) (%)	MAD (mm)	MAXD (mm)	Timesaving (%)	Speedup
Unedited 0	94.35 $\pm$ 7.30	91.38 $\pm$ 4.46	1.08 $\pm$ 0.42	3.39 $\pm$ 0.88	-17.79	0.85 $\times$
Unedited 1	92.77 $\pm$ 7.61	89.58 $\pm$ 2.22	1.35 $\pm$ 0.43	4.14 $\pm$ 0.95	24.22	1.32 $\times$
Unedited 2	92.19 $\pm$ 11.89	88.57 $\pm$ 4.57	1.52 $\pm$ 0.40	4.61 $\pm$ 0.86	33.87	1.51 $\times$
Unedited 3	90.58 $\pm$ 15.23	82.86 $\pm$ 6.52	2.00 $\pm$ 0.46	5.69 $\pm$ 1.03	39.00	1.64 $\times$
Unedited 4	88.48 $\pm$ 16.42	77.56 $\pm$ 8.04	2.34 $\pm$ 0.56	6.45 $\pm$ 1.09	41.59	1.71 $\times$
Unedited 5	85.15 $\pm$ 17.95	71.59 $\pm$ 9.91	2.74 $\pm$ 0.68	7.12 $\pm$ 1.11	44.45	1.80 $\times$

**Fig. 1** Prostate MR image sequence for a sample volume dataset. The *solid labels* represent the consensus contours for the prostate gland derived from the manual contours of five expert users



**Fig. 2** Segmentation results for the sample volume dataset shown in Fig. 1 with the sequential registration-based segmentation (SRS) algorithm for a configuration where two slice contours remain unedited between each pair of manually contoured slices. The segmentation results are shown for rigid registration (*dashed red line*), affine registration (*dotted blue line*), and demon (nonrigid) registration (*dashed-dotted green line*). The *solid line labels* are the ground-truth (consensus) contours created by manual contours of five expert users



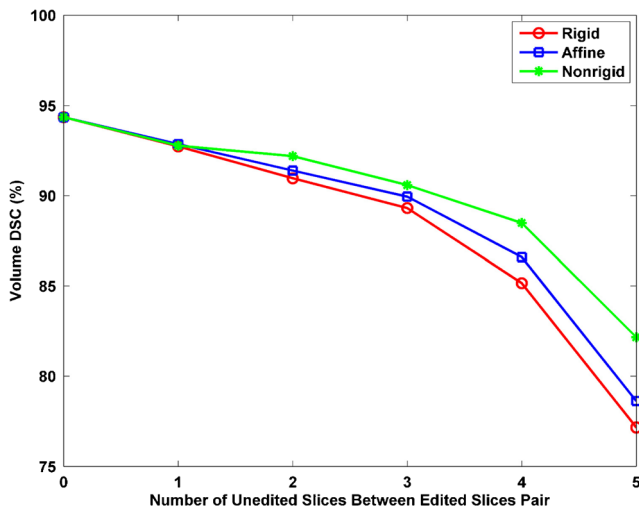


**Fig. 3** Average volume DSCs of the SRS algorithm with respect to the number of unedited slices between manually contoured slices in a prostate MR volume

user interacts with the segmentation algorithm to improve the accuracy. The SRS algorithm requires user interaction to contour a slice and depending on the selected configuration, one or more slices can be skipped before manually contouring the next slice. The proposed algorithm exploits the inter-slice similarity of the images in a volume dataset and eliminates the need for an atlas, which minimizes the computational costs. We verified the performance of the algorithm using 15 datasets of prostate MR images with 5 radiation oncologists contouring the images. Different configurations of the algorithm yielded different performance results. For example, the SRS algorithm with rigid registration produced results with an average volume DSC of 89.31 %, which is comparable to the intra-user agreement level (i.e., 89.82 %) while reducing the contouring time by 70 % (speedup factor of 3.33×). The

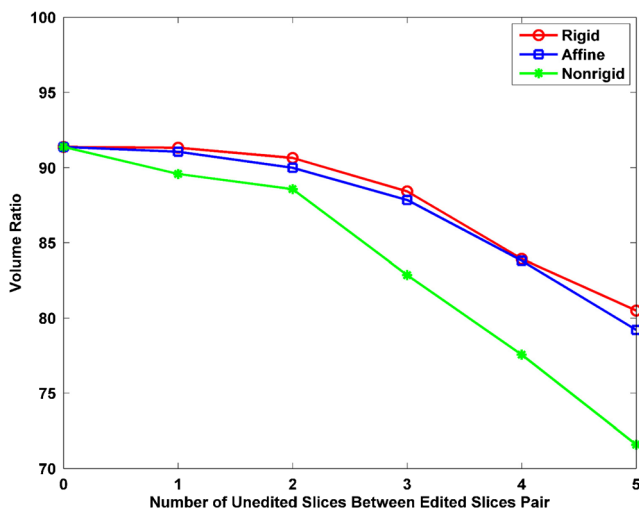


**Fig. 4** Average volume ratios of SRS algorithm with respect to the number of unedited slices between manually contoured slices in a prostate MR volume

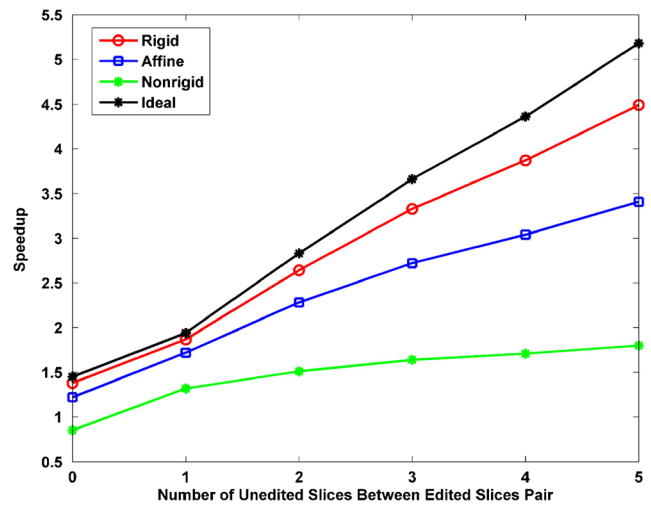


**Fig. 5** Speedup factors achieved by SRS algorithm using rigid, affine, and nonrigid registration methods. “Ideal” represents the speedup factor when the computational time of SRS is negligible compared to manual contouring time

timesaving in contouring, which is a high-demand daily task in hospitals, can translate to higher patient throughput in healthcare system.

**Acknowledgments** The authors would like to thank FedDev Ontario, Canada, for supporting this research. The authors would also like to thank Segasist Technologies for providing DICOM datasets and experts’ markings.

**References**

1. Prostate Cancer Canada, “What’s your number? Prostate cancer Canada annual report.,” [www.prostatecancer.ca](http://www.prostatecancer.ca), 2010
2. Smith WL, et al: “Prostate volume contouring: a 3D analysis of segmentation using 3DTRUS, CT, and MR”. *Int J Radiat Oncol Biol Phys* 67(4):1238–1247, 2007
3. Steenbakkers RJ, Deurloo KE, Nowak PJ, Lebesque JV, van Herk MM, Rasch CR: “Reduction of dose delivered to the rectum and bulb of the penis using MRI delineation for radiotherapy of the prostate.”. *Int J Radiat Oncol Biol Phys* 57:1269–1279, 2003
4. Jonsson JH, Karlsson MG, Karlsson M, Nyholm T: “Treatment planning using MRI data: an analysis of the dose calculation accuracy for different treatment regions”. *Radiat Oncol* 5:62, 2010. doi: 10.1186/1748-717X-5-62
5. Klein S, van der Heide UA, Raaymakers BW, Kotte ANTJ, Staring M, Pluim JPW, “Segmentation of the prostate in MR images by atlas matching,” *IEEE Conf. Biomed. Imaging*, 2007, pp.1300 - 1303
6. Klein S, van der Heide UA, Lips IM, van Vulpen M, Staring M, Pluim JPW: Automatic segmentation of the prostate in 3D MR images by atlas matching using localized mutual information. *Med Phys* 35:1407–1417, 2008
7. Dowling J, Fripp J, Greer P, Patterson J, Our selin S, Salvador O: “Automatic atlas-based segmentation of the prostate: A MICA 2009 Prostate segmentation challenge entry”, In: *Workshop in Med. Image Compute. Assist. Intern*, 2009, pp. 1724
8. Langerak TR, van der Heide UA, Kotte ANTJ, Vieregger MA, van Vulpen M, Pluim JPW: Label Fusion in Atlas-Based Segmentation

- Using a Selective and Iterative Method for Performance Level Estimation (SIMPLE). *IEEE Trans Med Imaging* 29:2000–2008, 2010
9. Martin S, Trocraz J, Daanen V: Automated segmentation of the prostate in 3D MR images using a probabilistic atlas and a spatially constrained deformable model. *Med Phys* 37:1579–1590, 2010
  10. Warfield SK, Zou KH, Wells WM: Simultaneous Truth and Performance Level Estimation (STAPLE): An Algorithm for the Validation of Image Segmentation. *IEEE Trans Med Imaging* 23: 903–921, 2004
  11. Cheng R, Turkbey B, Senseney J, Bernardo M, Bokinsky A, Gandler W, McCreedy E, Pohida T, Choyke P, McAuliffe MJ: “2D registration guided models for semi-automatic MRI prostate segmentation”. *Proc. SPIE 8669, Medical Imaging 2013: Image Processing*, 86692V, 2013, doi:10.1117/12.2006225.
  12. Radiation therapy oncology group, “contouring atlases,.” [www.rtog.org/CoreLab/ContouringAtlases.aspx](http://www.rtog.org/CoreLab/ContouringAtlases.aspx).
  13. Langer DL, van der Kwast TH, Evans AJ, Trachtenberg J, Wilson BC, Haider MA: Prostate cancer detection with multi-parametric MRI: Logistic regression analysis of quantitative T2, diffusion-weighted imaging, and dynamic contrast-enhanced MRI. *Magn Reson Imaging* 30:327–334, 2009
  14. Hentschel B, Oehler W, Strau D, Ulrich A, Malich A: Definition of the CTV Prostate in CT and MRI by Using CT-MRI Image Fusion in IMRT Planning for Prostate Cancer. *Strahlenther Onkol* 187(3): 183–190, 2011. doi:10.1007/s00066-010-2179-1
  15. Maintz JBA, Viergever MA: A survey of medical image registration. *Med Image Anal* 2:1–36, 1998
  16. Brown LG: A survey of image registration techniques. *ACM Comput Surv* 24:325–376, 1992
  17. Thirion JP: Image matching as a diffusion process: an analogy with Maxwell’s demons. *Med Image Anal* 196:243–260, 1998
  18. Guimond A, Roche A, Ayache N, Meunier J: Three-dimensional multimodal brain warping using the demons algorithm and adaptive intensity corrections. *IEEE Trans Med Imaging* 20(1):58–69, 2001
  19. Wang H, Dong L, O’Daniel J, Mohan R, Garden AS, Ang KK, Kuban DA, Bonnen M, Chang JY, Cheung R: Validation of an accelerated ‘demons’ algorithm for deformable image registration in radiation therapy. *Phys Med Biol* 50(12):2887–2905, 2005
  20. Kroon DJ, “Multimodality nonrigid demon algorithm image registration”, MatlabCentral, [www.mathworks.com/matlabcentral/fileexchange/21451-multimodality-non-rigid-demon-algorithm-image-registration](http://www.mathworks.com/matlabcentral/fileexchange/21451-multimodality-non-rigid-demon-algorithm-image-registration).
  21. Martin S, Rodrigues G, Patil N, Bauman G, D’Souza D, Sexton T, Palma D, Louie AV, Khalvati F, Tizhoosh HR, Gaede S: “Multiphase validation of atlas-based automatic and semiautomatic segmentation strategies for prostate MRI”. *Int J Radiat Oncol Biol Phys* 1(85(1)):95–100, 2013. doi:10.1016/j.ijrobp.2011.07.046
  22. Al-Qunaieer FS, Tizhoosh HR, Rahnamayan S: Multi-resolution level sets with shape priors: a validation report for 2D segmentation of prostate gland in T2W MR images. *J Digit Imaging* 27(6):833–847, 2014
  23. Khalvati F, Salmanpour A, Rahnamayan S, Rodrigues G, Tizhoosh HR: “Inter-slice bidirectional registration-based segmentation of the prostate gland in MR and CT image sequences”. *Med Phys* 40(12):123503-1–123503-11, 2013